Cluster kinematics and stellar rotation in NGC 419 with MUSE and adaptive optics

S. Kamann, N. Bastian, T. -O. Husser, S. Martocchia, C. Usher, M. den Brok, S. Dreizler, A. Kelz, D. Krajnović, J. Richard, et al.

Monthly Notices
of the
ROYAL ASTRONOMICAL SOCIETY

MNRAS **480,** 1689–1695 (2018)
Advance Access publication 2018 July 24

doi:10.1093/mnras/sty1958

Cluster kinematics and stellar rotation in NGC 419 with MUSE and adaptive optics

S. Kamann,[1★] N. Bastian,[1] T.-O. Husser,[2] S. Martocchia,[1] C. Usher,[1] M. den Brok,[3] S. Dreizler,[2] A. Kelz,[3] D. Krajnović,[3] J. Richard,[4] M. Steinmetz,[3] and P. M. Weilbacher[3]

[1]*Astrophysics Research Institute, Liverpool John Moores University, 146 Brownlow Hill, Liverpool L3 5RF, UK*
[2]*Institut für Astrophysik, Georg-August Universität, Friedrich-Hund-Platz 1, D-37077Göttingen, Germany*
[3]*Leibniz-Institute for Astrophysics (AIP), An der Sternwarte 16, D-14482 Potsdam, Germany*
[4]*Univ Lyon, Univ Lyon1, Ens de Lyon, CNRS, Centre de Recherche Astrophysique de Lyon UMR5574, F-69230 Saint-Genis-Laval, France*

Accepted 2018 July 19. Received 2018 July 12; in original form 2018 March 28

ABSTRACT

We present adaptive optics (AO)-assisted integral-field spectroscopy of the intermediate-age star cluster NGC 419 in the Small Magellanic Cloud. By investigating the cluster dynamics and the rotation properties of main-sequence turn-off (MSTO) stars, we demonstrate the power of AO-fed MUSE observations for this class of objects. Based on 1 049 radial velocity measurements, we determine a dynamical cluster mass of $1.4 \pm 0.2 \times 10^5\,M_\odot$ and a dynamical mass-to-light ratio of 0.67 ± 0.08, marginally higher than simple stellar population predictions for a Kroupa initial mass function. A stacking analysis of spectra at both sides of the extended MSTO reveals significant rotational broadening. Our analysis further provides tentative evidence that red MSTO stars rotate faster than their blue counterparts. We find average $V\sin i$ values of 87 ± 16 and $130 \pm 22\,\mathrm{km\,s^{-1}}$ for blue and red MSTO stars, respectively. Potential systematic effects due to the low-spectral resolution of MUSE can reach $30\,\mathrm{km\,s^{-1}}$ but the difference in $V\sin i$ between the populations is unlikely to be affected.

Key words: instrumentation: adaptive optics – techniques: imaging spectroscopy – stars: kinematics and dynamics – stars: rotation – galaxies: star clusters: individual: NGC 419.

1 INTRODUCTION

One peculiar feature of young and intermediate age (<2 Gyr) massive clusters in the Large/Small Magellanic Cloud (LMC/SMC) is that they display extended main-sequence turn-off (MSTO). The origin of this feature has been the subject of much debate in recent years, with the main explanations being either age spreads of 10s to 100s of Myr within the clusters (e.g. Mackey et al. 2008; Goudfrooij et al. 2014) or a spread in stellar rotation rates (Bastian & de Mink 2009; Brandt & Huang 2015; Niederhofer et al. 2015), or both (Dupree et al. 2017). If massive clusters were shown to host such large age spreads, our view of the formation and early evolution of such objects would need to be radically redefined (Portegies Zwart, McMillan & Gieles 2010; Bastian & Lardo 2017). If, on the other hand, massive clusters hosted stars with a wide range of rotational velocities (from non-rotating to near-critical rotation), models predict a strong correlation between the colour and the projected rotation velocity of a star (e.g. Georgy et al. 2014). In Bastian et al. (2018), we recently showed that the predicted correlation is in good agreement with the measured rotation velocities in the 800 Myr old open cluster NGC 2818.

Additional questions remain about the global kinematics of massive clusters. Recent studies have suggested that massive clusters display significant global rotation, at young (Hénault-Brunet et al. 2012), intermediate (Davies et al. 2011; Mackey et al. 2013), and old ages (e.g. Kamann et al. 2018). This raises questions about the initial range and the age evolution of V/σ. In order to address this, large samples of clusters at all evolutionary stages need to be surveyed.

Finally, massive stellar clusters routinely serve as calibration sources in population synthesis studies because their integrated properties (e.g. mass-to-light ratios and their integrated spectra/colours) can be linked directly to the known underlying (resolved) stellar population. NGC 419, at an age of ∼1.5 Gyrs (Glatt et al. 2008), lies at an age where integrated properties are particularly insecure, due to the uncertainties in modelling the stellar evolutionary phases of stars that are dominating the light (e.g. Girardi et al. 2013). By measuring the mass-to-light ratio in such a cluster, strict constraints on simple stellar population models can be obtained.

In this work, we demonstrate how the new MUSE capabilities (e.g. Leibundgut et al. 2017) can help answering the aforementioned questions, even with relatively short exposure times of around 1 h. To this aim, we exploit MUSE observations of NGC 419, performed during the commissioning of its new adaptive optics (AO) system.

★ E-mail: s.kamann@ljmu.ac.uk

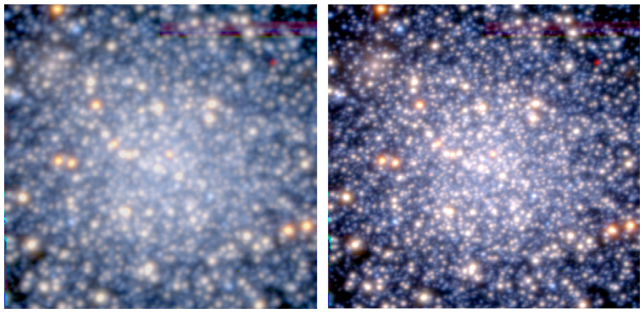

Figure 1. SDSS *gri* colour images of NGC 419, created from MUSE cubes without (*left*) and with (*right*) AO support, observed back-to-back. Each image is $1' \times 1'$ in size, the halflight radius of NGC 419 is 28 arcsec (Glatt et al. 2009). North is up; east is left.

NGC 419 has one of the most extended MSTOs observed to date and we use the data to measure the stellar rotation rates along the MSTO. In addition, we infer the global kinematics of the cluster and measure the dynamical mass-to-light ratio.

2 OBSERVATIONS AND DATA REDUCTION

The data were taken on the night of 2017 July 14 during the second commissioning run of AOF/GALACSI (La Penna et al. 2016; Arsenault et al. 2017), the new AO system for MUSE (Bacon et al. 2010). In total, eight exposures of 600 s each were taken. To verify the image quality improvement caused by the AO, the first four exposures were alternated between open and closed AO loop. The remaining four exposures were taken with closed loop.

We employed version 2.1.1 of the official MUSE pipeline (Weilbacher et al. 2014) to reduce the data. It differs from previous versions mainly by the added support for the AO mode and we refer the interested reader to, e.g. Kamann et al. (2018), for details on the data reduction process. From each science exposure, we created a flux calibrated data cube with the night sky subtracted. In Fig. 1, we compare re-constructed images from MUSE data cubes observed with and without AO support. The improvement in image quality delivered by GALACSI is nicely visible. The extremely red source visible in the north western corner of both cubes is an asymptotic giant star with extreme mass loss, originally discovered by Tanabé et al. (1997).

We combined the six AO exposures into our final data cube. To account for clouds passing during the observations, we adapted the exposure time of each cube to its flux level relative to the first exposure.

3 DATA ANALYSIS

We used our dedicated extraction code for integral field data described in Kamann, Wisotzki & Roth (2013) to extract stellar spectra from the data cube of NGC 419. As reference photometry catalogue, we used the data from the study of Martocchia et al. (2017). It includes *HST*/ACS and WFC3 magnitudes ranging from the UV to the near-infrared. Some bright stars that were found to be missing in the *HST* data because of saturation were added using coordinates and magnitudes from *Gaia* data release one (Gaia Collaboration 2016a,b).

We ran the source extraction on a combined cube created from the six AO exposures and on all individual exposures. The latter allowed us to get an idea of how the AO affects the point spread function (PSF). For the two exposures shown in Fig. 1, the full width at half-maximum (FWHM) of the Moffat profile improved from 0.74 arcsec (0.89 arcsec) to 0.35 arcsec (0.54 arcsec) at 8000 Å (5000 Å) when using the AO. At the same time we observed a decrease in β (which measures the kurtosis of a Moffat profile) from 2.8 (3.6) to 1.8 (2.2). This agrees with the general trend that the enhanced AO resolution comes at the price of pronounced PSF wings. Still, it is remarkable that even at the blue end of the wavelength range, the AO significantly improves the spatial resolution of MUSE. This also affects the number of resolvable stars. The number of extracted spectra increased by from 2 254 in the non-AO exposure to 5015 in the AO exposure. In addition, the average S/N of spectra extracted from both exposures improved by a factor of 1.7.

We further used the combined data cube to inspect the spatial behaviour of the PSF. AO observations often suffer from a degradation of the image quality with increasing distance to the natural guide star. As GALACSI additionally uses four laser guide stars that are placed around the MUSE field of view, spatial variations are expected to be small. Still, stronger variations could potentially affect the source extraction as it assumes the PSF to be constant across the field of view. We selected ∼50 reasonably bright and isolated stars distributed across the field of view. Each star was fitted with a single elliptical Moffat profile. In order to minimize the impact of nearby stars, the fit was performed iteratively and after each iteration nearby stars were subtracted using the current PSF model. The results of this analysis are summarized in Fig. 2. Overall, the variation of the PSF across the field of view seems to be small. The star-to-star scatter in the FWHM is of the order of 10 per cent, while it seems to be larger for β. However, a significant fraction of the scatter can be attributed to stars with low S/N and hence poorly constrained fits. No systematic variation is found with respect to the distance or position angle towards the natural guide star.

We find the PSF to be slightly elliptical, with a mean fitted ellipticity of $e = 0.07 \pm 0.04$. While the position angles of the semimajor axes seem to be well aligned, they are not directed towards the guide star as one would expect in AO observations that only use a natural guide star (cf. Fig. 2). We conclude that the AO does not introduce significant PSF variations across the field of view of MUSE that could affect the extraction of the stellar spectra.

In total, we extracted spectra for 5 538 stars over a wide range of signal-to-noise ratios (S/Ns). In the following, we will only use the spectra that were extracted with a S/N > 5 per pixel (averaged over the full spectrum), which we consider the minimum requirement for any analysis. Applying this cut results in a sample of 3 321 stars with useful spectra (60 per cent of the parent sample). Their distribution across the colour-magnitude diagram of NGC 419 is shown in Fig. 3. The faintest stars with spectra passing the S/N cut are situated about 2 mag below the MSTO while spectra of stars at the MSTO were extracted with a S/N ∼ 10.

4 DYNAMICAL CLUSTER MASS

To obtain radial velocities for our spectra, we cross correlated them against synthetic PHOENIX templates from the library of Husser et al. (2013). As a consequence of the broad range in S/N of the extracted spectra, however, not every spectrum allows for a reliable radial velocity measurement. Besides the S/N, we also used the height of the normalized cross-correlation peak (parametrized by the value r as defined by Tonry & Davis 1979) and only considered results from spectra where S/N > 5 and $r > 4$ were simultaneously fulfilled.

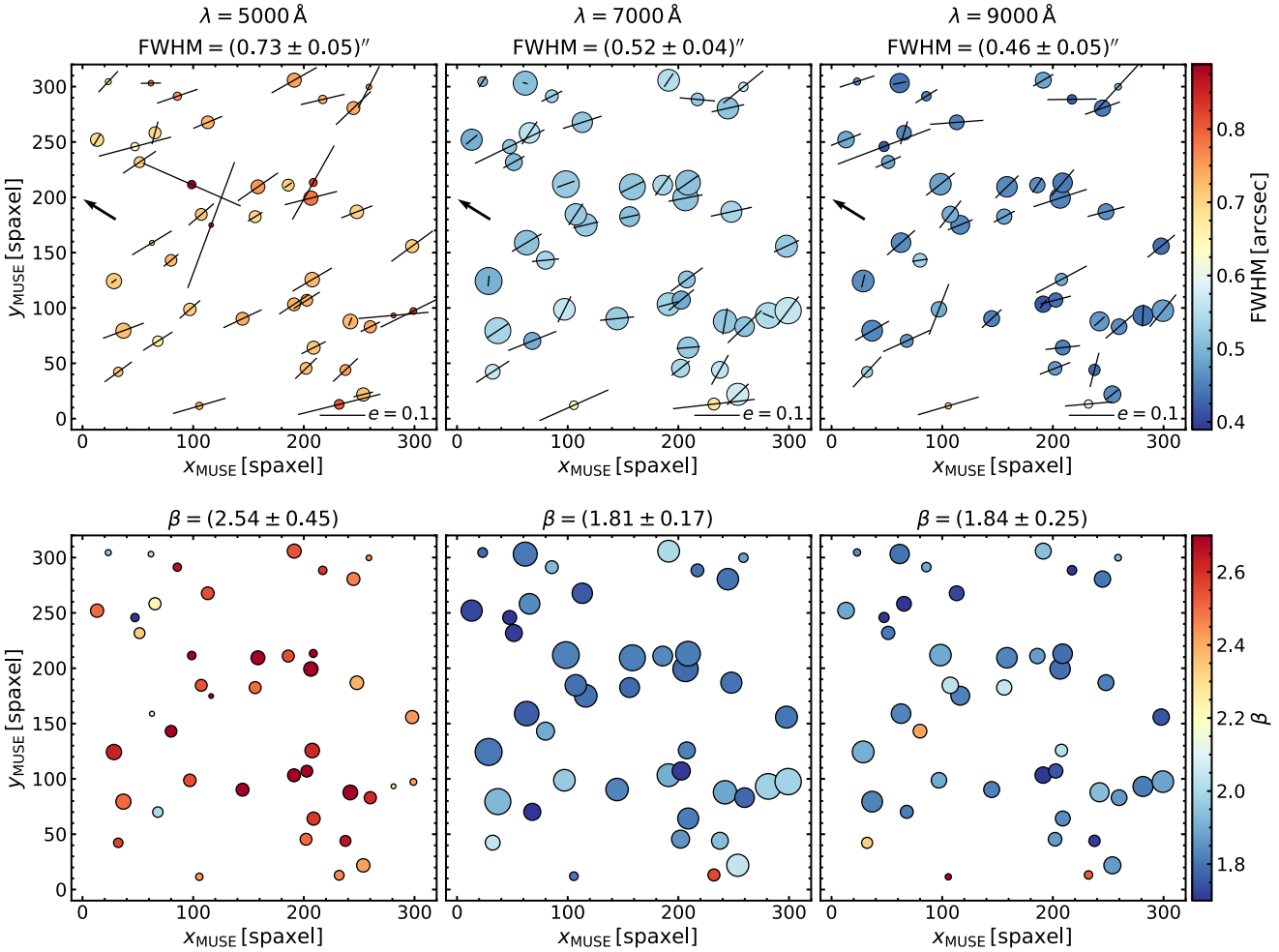

Figure 2. Variation of the MUSE AO-PSF with wavelength and across the field of view. The panels show the values of the FWHM (*top*) and β (*bottom*) obtained in single PSF fits of bright stars at 5000 Å (*left*), 7000 Å (*middle*), 9000 Å (*right*) as a function of the stars positions in the MUSE cube. Mean values and standard deviations of the parameters are provided at the top of each panels. The sizes of the circles scale with the S/N of the stars at the provided wavelengths. In the top panel, black lines indicate the ellipticities and the position angles of the best-fitting PSF models. The length of the lines scales linearly with ellipticity as indicated in the bottom right corner of each panel. The direction towards the natural guide star is indicated by a black arrow.

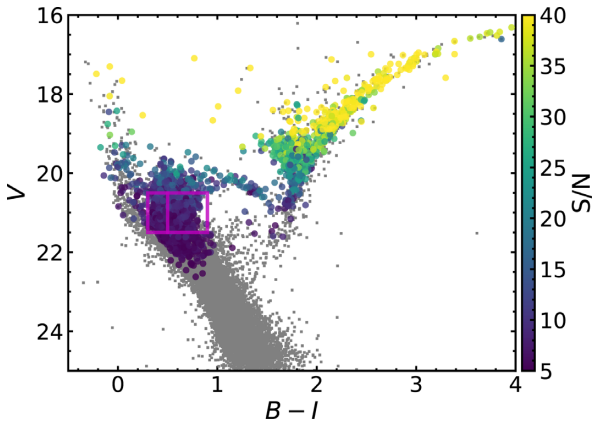

Figure 3. *HST* ($B - I$, V) colour magnitude diagram of NGC 419. Stars for which spectra with S/N > 5 were extracted from the MUSE data are colour coded according to the spectral S/N as indicated by the colour bar to the right. The purple boxes indicate the selection boxes for the red and blue MSTO stars, respectively.

To investigate the internal dynamics of star clusters, it is further crucial to properly calibrate the uncertainties of the measured radial velocities. A systematic over- or underestimation of the uncertainties would result in a bias in the measured velocity dispersion. As outlined in Section 3, besides the combined cube we also analysed the individual AO exposures. They provided us with multiple independent spectra for the majority of the stars in our sample. Following our previous work (e.g. Husser et al. 2016), we scaled the uncertainties returned by the cross-correlation routine for the individual spectra such that they were consistent with the differences in the radial velocities measured using spectra of the same stars. To account for possible trends with the S/N, the calibration was carried out in five S/N bins. The correction factors we found were around 10 per cent. For each star, we finally obtained its radial velocity and the associated uncertainty as the inverse-variance weighted mean and variance of the individual measurements. As expected, the measurement uncertainties strongly scale with the brightnesses and spectral types of the stars. Down the red giant branch, the average velocity uncertainties increase from 1 to 7 km s^{-1}. Along the main sequence, the stars are hotter and hence their spectra show fewer and broader lines. Accordingly, their radial velocities are less well defined, with

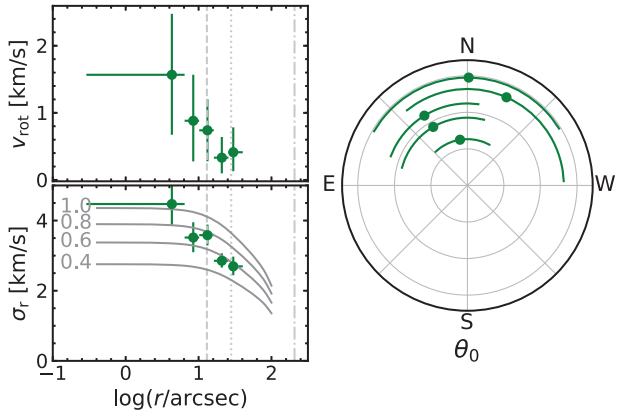

Figure 4. Internal dynamics of NGC 419 as determined from the MUSE data. The left-hand panels show the amplitude of the rotation field (*top*) and velocity dispersion (*bottom*) as a function of distance to the cluster centre, the behaviour of the axis angle of the rotation field is shown in the right-hand panel. The dispersion profile is compared to the predictions of spherical isotropic Jeans models with different *V*-band mass-to-light ratios, ranging from 0.4 × solar to 1.0 × solar (in steps of 0.2). Further, we show the core (dashed line), half-light (dotted line), and truncation radius (dash-dotted line) from the structural analysis of Glatt et al. (2009).

typical uncertainties ranging from 15 km s^{-1} at the tip of the MSTO to 35 km s^{-1} for the faintest stars in our sample. In view of the expected velocity dispersion of NGC 419 of 5 km s^{-1}, we excluded all stars with uncertainties > 10 km s^{-1} from the analysis of the cluster dynamics. This left us with 1049 measurements, obtained mainly from stars on the red giant branch.

The dynamics of the cluster was analysed using the same approach as in Kamann et al. (2018). It finds the maximum-likelihood solution for the intrinsic dispersion and the rotation field of the cluster given the data. Further, we used the Markov chain Monte Carlo (MCMC) approach of Foreman-Mackey et al. (2013) to obtain confidence intervals for the measured quantities. The formal uncertainties provided in the following are the 16th and 84th percentiles of the parameter distributions obtained from the MCMC walkers.

From an analysis of the full sample, we obtained a systemic radial velocity of NGC 419 of $v_{sys} = 190.5 \pm 0.2$ km s^{-1} which is in good agreement with 188.3 ± 0.9 km s^{-1}, obtained by Dubath, Meylan & Mayor (1997) from an integrated spectrum. The analysis further yielded a velocity dispersion of 3.1 ± 0.2 km s^{-1} and a rotation amplitude of 0.7 ± 0.2 km s^{-1}. The rotation axis is aligned approximately in north–south direction, with a position angle of 13 ± 17 degrees. Only one per cent of the MCMC samples have a rotation amplitude below the uncertainty quoted above, indicating a low probability for a non-rotating cluster.

For further analyses, we split our data into radial bins (each containing at least 100 measurements and covering a width of $\delta \log(r/1'') \geq 0.2$) and analysed them independently. Fig. 4 shows the results obtained for the individual bins. It is reassuring that for each of the radial bins, we obtain an angle of the rotation axis that is consistent with the value of 13 ± 17 degrees measured for the full sample. The rotation velocity seems to increase towards the centre of NGC 419, albeit the significance of this observation is low. If confirmed, this behaviour would be surprising. In their analysis of the LMC cluster NGC 1846, which has a similar age to NGC 419, Mackey et al. (2013) used the violent relaxation model of Lynden-Bell (1967) to describe the rotation profile. It predicts an increase of the rotation velocity with distance to the cluster centre inside the half-light radius. Most rotating globular clusters also show this behaviour, (e.g. Bianchini et al. 2013; Fabricius et al. 2014; Kamann et al. 2018). In addition, dedicated models for rotating globular clusters (e.g. Varri & Bertin 2012) predict an increase in the rotation velocity with radius as well, up to a maximum that is reached at a few half-light radii and beyond which the rotation velocity steadily decreases. However, our data lacks the spatial coverage for a detailed comparison to such models.

The velocity dispersion profile depicted in Fig. 4 further allows us to determine the mass-to-light ratio (M/L) and the dynamical mass of NGC 419. To this aim, we performed a multi-Gaussian expansion (MGE; see Cappellari 2002) of the surface brightness profile of NGC 419. We used the parametric representation of the surface brightness profile obtained by Carvalho et al. (2008) as input. Then we calculated isotropic, spherical Jeans models with different (constant) M/Ls using the code of Cappellari (2008). The velocity dispersion profiles predicted by Jeans models with representative M/Ls are included in Fig. 4. To find the most likely M/L given our data, we used the same maximum likelihood approach adopted by Merritt & Saha (1993) and Gerssen et al. (2002). It calculates a likelihood for each model under the assumption that each measured radial velocity is drawn from a Gaussian distribution which has a variance equal to the sum of squares of the measurement uncertainty and the velocity dispersion predicted by the model for the position of the star. Hence, it requires no binning of the data; the bins shown in Fig. 4 are used for displaying purposes only. This analysis yields a M/L in the *V*-band in solar units of 0.67 ± 0.06, where the 1σ confidence interval has been obtained using a likelihood ratio test. It does not account for uncertainties in the surface brightness profile determination. To get an idea of the uncertainty in the surface profile determination, we also used the King (1962) profile determined by Goudfrooij et al. (2014) as input to our Jeans modelling, which reduced the M/L of the best matching model by 0.05. The difference can be ascribed to an excess of light in the Goudfrooij et al. (2014) profile. Its numerical integration yields $m_V = 10.24$ compared to $m_V = 10.35$ for the Carvalho et al. (2008) profile. We add the offset in M/L of 0.05 in quadrature to our uncertainties which gives a final result of 0.67 ± 0.08. Our value is only slightly above the predictions for simple stellar populations based on a Kroupa (2002) initial mass function (IMF) at an age of 1.5 Gyr (Glatt et al. 2008). We obtain predictions of 0.48 ± 0.05 using MILES (Vazdekis et al. 2010), 0.50 ± 0.06 using FSPS (Conroy, Gunn & White 2009; Conroy & Gunn 2010), 0.62 ± 0.04 using the 2016 version of the Bruzual & Charlot (2003) models, and 0.53 ± 0.03 using the models of Maraston (2005).

As mentioned above, numerical integration of the profile by Carvalho et al. (2008) results in an apparent cluster brightness of $m_V = 10.35$. In combination with a distance modulus of NGC 419 of $(m - M) = 18.85 \pm 0.03$ (Goudfrooij et al. 2014), we obtain a dynamical cluster mass of $1.4 \pm 0.2 \times 10^5$ M$_\odot$. This is lower than the value of $2.4 \pm 0.4 \times 10^5\, M_\odot$ determined by Goudfrooij et al. (2014), who converted the measured light to mass by adopting an simple stellar population model. However, Goudfrooij et al. (2014) assumed a Salpeter (1955) IMF in their stellar population synthesis and mentioned that the usage of a Kroupa (2002) IMF instead would lower their masses by a factor of ∼1.6, explaining most of the discrepancy to our measurement. Hence, our study suggests that a Kroupa (2002) IMF yields a better representation of the intrinsic IMF of NGC 419.

We note that the dispersion measurements in Fig. 4 suggest a slightly steeper radial profile than the Jeans models. The reason

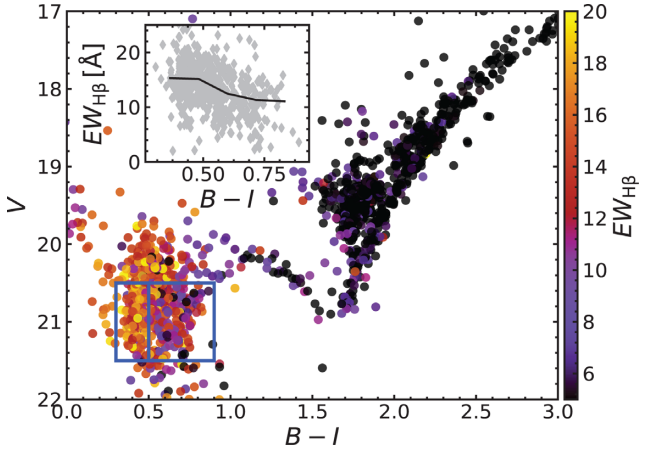

Figure 5. CMD of NGC 419, colour-coded by the measured equivalent width of H β. The inset shows the equivalent width variation as a function of $(B - I)$-colour for stars at the MSTO of NGC 419 (highlighted by the blue boxes), with the running median indicated by a black solid line.

for this is currently unclear, as anisotropy, a radially varying M/L, or binary stars could all affect our analysis. However, a detailed exploration of all mentioned effects is not possible with the current data.

5 STELLAR ROTATION AND THE EXTENDED MSTO

Fig. 3 shows that our sample contains a good fraction of stars around the MSTO of NGC 419. According to the oldest models in the grid of Georgy et al. (2014, 1 Gyr), one would expect the projected rotation velocity $V\sin i$ to gradually increase with colour if the extended MSTO was caused by stellar rotation. Hence, we defined two selection boxes, covering the red and the blue side of the MSTO as indicated in Fig. 3. The division between the two boxes at $B - I = 0.5$ was chosen such that each of them contained a comparable number of stars from our sample (∼250).

We first determined the equivalent width of the H β line in the spectra of the selected stars. Given the comparable age and evolutionary status of the stars, H β should be sensitive to changes of the effective temperature. As visible in Fig. 5, we find the equivalent width of H β to decrease with increasing $B - I$ colour. The mean values for the two sub-samples are 15.2 ± 0.3 and 12.5 ± 0.3 Å, respectively. At about 7 500 K (the expected temperature for MSTO stars in NGC 419), the difference in equivalent width corresponds to a difference in effective temperature of 300–400 K.

Measuring stellar rotation rates is challenging because of the low-spectral resolution of MUSE and the relatively low S/N of the MSTO stars in these commissioning data. To circumvent the latter problem, we made use of our large sample size and averaged the normalized spectra of the stars that fell in either of the two selection boxes highlighted in Fig. 3. Uncertainties for the combined spectra were determined via bootstrapping of the input spectra. The different radial velocities of the stars we consider will spuriously broaden the stacked spectra. While our analysis of Section 4 provided us with radial velocities also for the MSTO stars, their uncertainties are considerable. For this reason, we did not correct the individual spectra for the measured radial velocities, but only for the systemic velocity of NGC 419, $v_{\rm sys} = 190.5\,{\rm km\,s^{-1}}$, determined in Section 4. The intrinsic velocity dispersion of NGC 419 of $\lesssim$4 km s^{-1} is much lower than the expected rotational velocities, hence the radial velocities of the cluster stars should not affect the following analyses. We further verified that the contamination from SMC field stars in our selection boxes is low, $\lesssim$10 per cent, by using the same method described in Martocchia et al. (2017). The influence of field stars was further reduced by only accepting stars with a reliable velocity measurement within 30 km s^{-1} of the systemic velocity of NGC 419.

The two combined spectra are depicted in the upper panel of Fig. 6. The S/N determined in both cases is ∼180. Both spectra are dominated by the strong H β and H α lines as well as the Paschen series of hydrogen. The insets in the upper panel of Fig. 6 zoom in on the Mg*b* triplet and the strongest lines of the Ca II triplet. These lines are the strongest apart from the neutral hydrogen lines, over which they have the advantage of a much lower line width. A visual comparison of the two spectra does not reveal a clear indication that the red MSTO spectrum has broader lines (corresponding to a higher rotation velocity) than the blue MSTO spectrum. However, one has to keep in mind the rather low-spectral resolution of MUSE and the temperature difference between the red and blue MSTO stars, as the higher temperature of the latter stars may counterbalance a higher rotation velocity of the former. Therefore, any conclusion on the rotation velocities across the MSTO requires a more detailed analysis, which we carry out below.

In the absence of isolated lines suited for direct rotation measurements, we obtained rotation velocities for the combined spectra as follows. First, the data were analysed with the spectral synthesis code of Husser et al. (2016) under the assumption that $V\sin i = 0$, yielding the stellar parameters listed in Table 1.[1] The temperature difference of ∼250 K that we obtained is in general agreement with that predicted from the difference in H β equivalent width. Both averaged spectra are fitted with a surface gravity that is consistent with main-sequence stars and a metallicity [*M*/*H*] that is in good agreement with photometric estimates of the cluster metallicity ([Fe/H] = −0.7; e.g. Martocchia et al. 2017).

A rotation velocity was finally obtained by applying rotational broadening according to the formula of Gray (2008)[2] to the templates in a least squares fit to the data. This yielded values of $V\sin i = 87 \pm 16\,{\rm km\,s^{-1}}$ and $130 \pm 22\,{\rm km\,s^{-1}}$ for the blue and red MSTO spectrum, respectively. The uncertainties were obtained by re-noising the spectra using the uncertainties obtained as outlined above and re-evaluating $V\sin i$.

Our analysis hence provides evidence for rotational broadening of both spectra and tentative evidence for an increase of the average $V\sin i$ towards the red side of the MSTO. To visualize the effect of the measured rotational broadening on MUSE spectra, we show in the lower panel of Fig. 6 two synthetic PHOENIX spectra. They have similar stellar parameters as obtained for the combined MSTO spectra and were broadened using the $V\sin i$ values obtained for the red and blue MSTO spectrum, respectively. The synthetic spectra were transformed to the MUSE spectral resolution and sampling. As was the case for the observed spectra depicted in the upper panel, a visual comparison does not reveal a stronger rotational broadening of the red template spectrum. Hence, to reveal stellar rotation at the spectral resolution of our data, we have to rely on an in-depth analysis as performed above. To further verify our $V\sin i$ values, we performed 1000 realizations in which we degraded the synthetic

[1] As explained in Husser et al. (2016), we denote metallicities measured from MUSE spectra by [*M*/*H*] instead of [Fe/H] to account for the fact that the values are based on a fit of the full spectrum instead of individual iron lines.

[2] Using the implementation in https://github.com/sczesla/PyAstronomy.

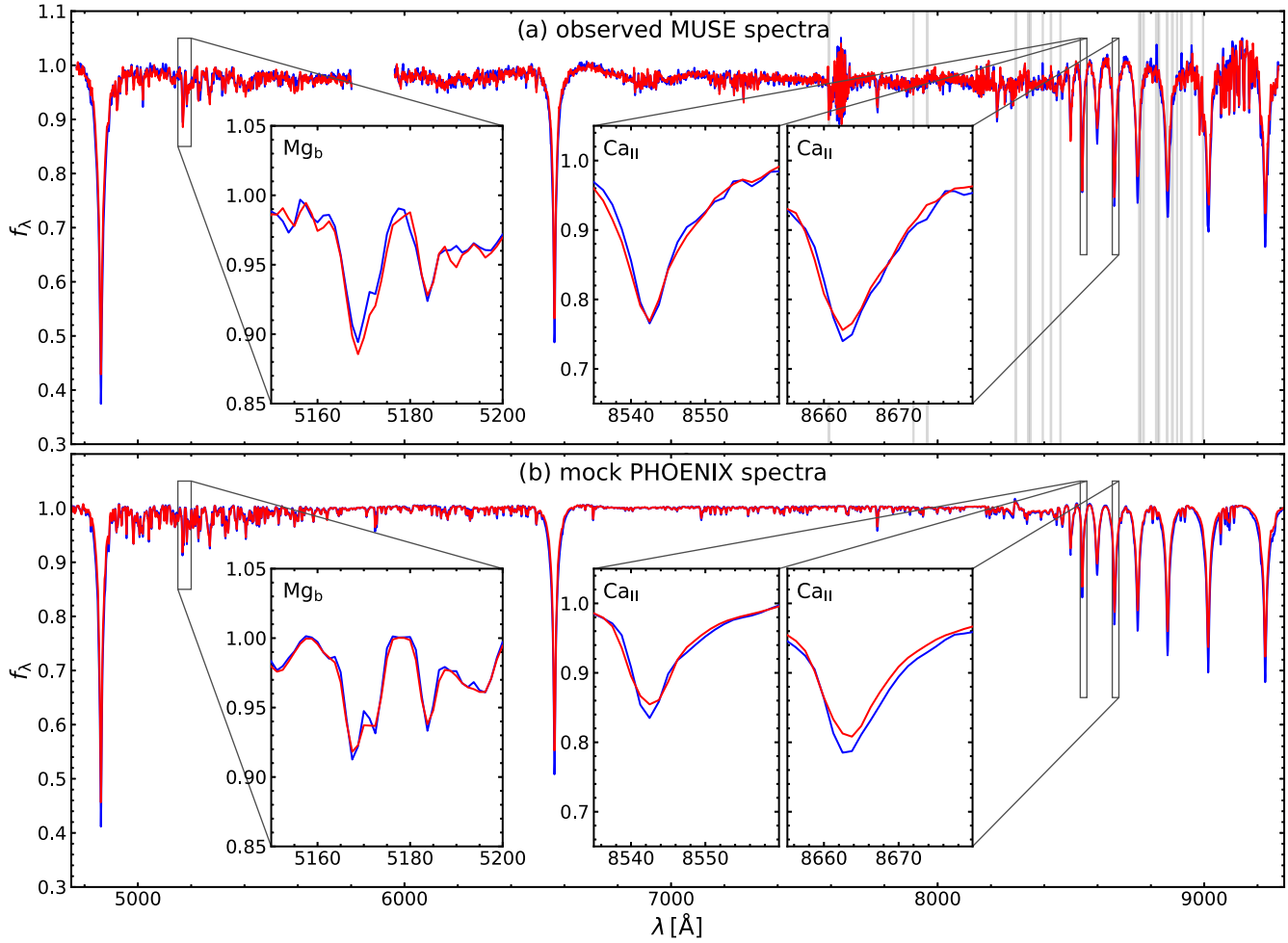

Figure 6. *(Top)* Comparison of combined MUSE spectra of MSTO stars in NGC 419 with $B - I < 0.5$ (blue) and >0.5 (red), created by combining the (normalized) spectra extracted for stars in the boxes highlighted in Fig. 3. The insets in the upper panel show a zoom to the Mg*b* triplet and to the strongest lines of the Ca II triplet. Grey-shaded areas indicate wavelength ranges affected by strong telluric emission lines. *(Bottom)* The same for synthetic PHOENIX templates with stellar parameters comparable to those obtained for the observed MSTO spectra. The spectra were transformed to the MUSE spectral resolution and sampling and broadened assuming $V \sin i$ values of 87 km s^{-1} (blue) and 130 km s^{-1} (red), respectively.

Table 1. Results of the spectral analysis of the combined MSTO spectra.

	Blue MSTO	Red MSTO
$T_{\rm eff}$ [K]	7690 ± 20	7420 ± 20
$\log g$	4.44 ± 0.03	4.41 ± 0.03
$[M/H]$	-0.67 ± 0.03	-0.74 ± 0.03

spectra shown in the lower panel of Fig. 6 to a random S/N between 1 and 200 and attempted to recover the input values of $V \sin i$. We found that above a S/N of 50, we are able to recover the input values to an accuracy within the confidence intervals quoted above.

While this simulation gives us an idea of the accuracy that we can achieve with MUSE spectra if a perfectly matching template is available, it does not account for potential mismatches between the observed spectra and the syntetic templates. We investigated the impact of such mismatches on our analysis by modifying the analysis on the synthetic templates such that the spectra used to recover $V \sin i$ were offset from the broadened templates in effective temperature (by 200 K), surface gravity (by 0.5 dex), and alpha-element abundance (by 0.4 dex). We found that such mismatches can indeed have a significant impact on the recovery of $V \sin i$. The offsets we measured were as large as ± 30 km s^{-1}. However, we did not encounter a situation where the recovered rotation for either of the spectra was consistent with zero. In addition, the systematics affected both spectra in the same sense, so that the difference in $V \sin i$ between the red and blue spectrum persisted. Hence, we conclude that systematic effects have a stronger effect on the absolute values of $V \sin i$ than on their relative difference which we consider robust.

6 DISCUSSION AND CONCLUSIONS

In a study of the rotation properties of A stars in the field, Royer et al. (2002) found an unimodal distribution, peaking at equatorial velocities between 100 and 200 km s^{-1}. While this is in general agreement with the (projected) rotation velocities we obtained in the analysis of the combined MSTO spectra, it is not obvious that A stars in clusters share the same rotation properties as their analogues in the field (see, e.g. Huang & Gies 2006; Wolff et al. 2007, for more massive stars). An important difference between the two populations is their age distributions, as the age-evolution of the rotation of A-stars can be quite complex (Zorec & Royer 2012).

Our analysis provides evidence that the stars on the red side of the main sequence rotate on average faster than their bluer counterparts, the difference in $V\sin i$ is $\sim$40 km s^{-1}. If we use the models of Georgy et al. (2014) for a 1 Gyr cluster and assume an isotropic distribution of inclination angles, we obtain a difference of $\sim$100 km s^{-1}. Our recent work on the Galactic open cluster NGC 2818 (Bastian et al. 2018) has shown that these models accurately describe the relation between colour and $V\sin i$ across the MSTO of this 0.8 Gyr old cluster. However, as 1 Gyr is the maximum age currently covered in the models and NGC 419 is still 0.5 Gyr older, there are no models that we can directly compare to our results without extrapolation to older ages. It would be an important step forward to extend the evolutionary models to the age of NGC 419.

Finally, our analysis of the cluster dynamics yielded a dynamical mass-to-light ratio of 0.67 $\pm$ 0.08, slightly higher than the predictions of simple stellar population models and hints to the presence of rotation inside the cluster. The observation that clusters at all ages show rotation (e.g. Davies et al. 2011; Hénault-Brunet et al. 2012; Kamann et al. 2018) suggests that they form with significant angular momentum. A survey that traces the evolution of angular momentum across all cluster ages therefore promises to reveal crucial information about the formation of massive clusters. Our analysis of NGC 419 has shown that the combination of MUSE and AOs provides us with a powerful opportunity to do so.

ACKNOWLEDGEMENTS

We thank Roland Bacon, Joel Vernet, the MUSE team, and the staff at ESO for their efforts during the instrument commissioning and for making the data available to the community. SK, NB, and CU gratefully acknowledge funding from a European Research Council-consolidator grant (ERC-CoG-646928-Multi-Pop). AK und PMW acknowledge funding from Bundesministerium fuer Bildung und Forschung(BMBF)-Verbundforschung (grant 05A17BAA). This work made use of PyAstronomy and Astropy (Astropy Collaboration 2013). This study was based on public data released from the MUSE WFM-AO commissioning observations at the VLT Yepun (UT4) telescope under Programme ID 60.A-9100(G) and 60.A-9100(H).

REFERENCES

Astropy Collaboration, 2013, A&A, 558, A33
Arsenault R. et al., 2017, ESO Messenger, 168, 8
Bacon R. et al., 2010, in McLean I. S., Ramsay S. K., Takami H., eds, Ground-based and Airborne Instrumentation for Astronomy III, Vol. 7735. SPIE, Bellingham, p. 773508
Bastian N. J. et al., 2018, MNRAS, 00, 00
Bastian N., de Mink S. E., 2009, MNRAS, 398, L11
Bastian N., Lardo C., 2017, preprint (arXiv:1712.01286)
Bianchini P., Varri A. L., Bertin G., Zocchi A., 2013, ApJ, 772, 67
Brandt T. D., Huang C. X., 2015, ApJ, 807, 25
Bruzual G., Charlot S., 2003, MNRAS, 344, 1000
Cappellari M., 2002, MNRAS, 333, 400
Cappellari M., 2008, MNRAS, 390, 71
Carvalho L., Saurin T. A., Bica E., Bonatto C., Schmidt A. A., 2008, A&A, 485, 71
Conroy C., Gunn J. E., 2010, ApJ, 712, 833
Conroy C., Gunn J. E., White M., 2009, ApJ, 699, 486
Davies B., Bastian N., Gieles M., Seth A. C., Mengel S., Konstantopoulos I. S., 2011, MNRAS, 411, 1386
Dubath P., Meylan G., Mayor M., 1997, A&A, 324, 505
Dupree A. K. et al., 2017, ApJ, 846, L1
Fabricius M. H. et al., 2014, ApJ, 787, L26
Foreman-Mackey D., Hogg D. W., Lang D., Goodman J., 2013, PASP, 125, 306
Gaia Collaboration G., 2016a, A&A, 595, A1
Gaia Collaboration G., 2016b, A&A, 595, A2
Georgy C., Granada A., Ekström S., Meynet G., Anderson R. I., Wyttenbach A., Eggenberger P., Maeder A., 2014, A&A, 566, A21
Gerssen J., van der Marel R. P., Gebhardt K., Guhathakurta P., Peterson R. C., Pryor C., 2002, AJ, 124, 3270
Girardi L., Marigo P., Bressan A., Rosenfield P., 2013, ApJ, 777, 142
Glatt K. et al., 2008, AJ, 136, 1703
Glatt K. et al., 2009, AJ, 138, 1403
Goudfrooij P. et al., 2014, ApJ, 797, 35
Gray D. F., 2008, The Observation and Analysis of Stellar Photospheres, Cambridge Univ. Press, Cambridge.
Hénault-Brunet V. et al., 2012, A&A, 546, A73
Huang W., Gies D. R., 2006, ApJ, 648, 580
Husser T.-O., Wende-von Berg S., Dreizler S., Homeier D., Reiners A., Barman T., Hauschildt P. H., 2013, A&A, 553, A6
Husser T.-O. et al., 2016, A&A, 588, A148
Kamann S., Wisotzki L., Roth M. M., 2013, A&A, 549, A71
Kamann S. et al., 2018, MNRAS, 473, 5591
King I., 1962, AJ, 67, 471
Kroupa P., 2002, Science, 295, 82
La Penna P. et al., 2016, in Marchetti E., Close L. M., Véran J. P., eds, Adaptive Optics Systems V, Vol. 9909, SPIE, Bellingham, p. 99092Z
Leibundgut B. et al., 2017, ESO Messenger, 170, 20
Lynden-Bell D., 1967, MNRAS, 136, 101
Mackey A. D., Broby Nielsen P., Ferguson A. M. N., Richardson J. C., 2008, ApJ, 681, L17
Mackey A. D., Da Costa G. S., Ferguson A. M. N., Yong D., 2013, ApJ, 762, 65
Maraston C., 2005, MNRAS, 362, 799
Martocchia S. et al., 2017, MNRAS, 468, 3150
Merritt D., Saha P., 1993, ApJ, 409, 75
Niederhofer F., Georgy C., Bastian N., Ekström S., 2015, MNRAS, 453, 2070
Portegies Zwart S. F., McMillan S. L. W., Gieles M., 2010, ARA&A, 48, 431
Royer F., Gerbaldi M., Faraggiana R., Gómez A. E., 2002, A&A, 381, 105
Salpeter E. E., 1955, ApJ, 121, 161
Tanabé T. et al., 1997, Nature, 385, 509
Tonry J., Davis M., 1979, AJ, 84, 1511
Varri A. L., Bertin G., 2012, A&A, 540, A94
Vazdekis A., Sánchez-Blázquez P., Falcón-Barroso J., Cenarro A. J., Beasley M. A., Cardiel N., Gorgas J., Peletier R. F., 2010, MNRAS, 404, 1639
Weilbacher P. M., Streicher O., Urrutia T., Pécontal-Rousset A., Jarno A., Bacon R., 2014, in Manset N., Forshay P., eds, ASP Conf. Ser. Vol. 485, Astronomical Data Analysis Software and Systems XXIII, Astron. Soc. Pac., San Francisco, p. 451
Wolff S. C., Strom S. E., Dror D., Venn K., 2007, AJ, 133, 1092
Zorec J., Royer F., 2012, A&A, 537, A120

This paper has been typeset from a TEX/LATEX file prepared by the author.